Observational and model studies of the circulation in the Gulf of Tonkin, South China Sea

Yang Ding,[1,2] Changsheng Chen,[2,3] Robert C. Beardsley,[4] Xianwen Bao,[1] Maochong Shi,[1] Yu Zhang,[2] Zhigang Lai,[5] Ruixiang Li,[6] Huichan Lin,[2,3] and Nguyen T. Viet[7]

[1] Moored current measurements were made at one mooring site in the northern Gulf of Tonkin for about 1 year during 1988–1989. Analyses were performed to examine characteristics and variability of tidal and subtidal flows. Rotary spectra showed two peaks at diurnal and semidiurnal periods, with higher diurnal energy. Complex demodulations of diurnal and semidiurnal tidal currents indicated that the tidal current magnitudes varied significantly with seasons: more energetic in the stratified summer than in the vertically well-mixed winter. The observed subtidal currents were highly correlated with the surface wind in winter but not in summer; challenging the conceptual summertime anticyclonic circulation pattern derived using wind-driven homogenous circulation theory. The computed currents from a global ocean model were in good agreement with the observed currents. Similar to the current observations, the model-computed flow patterns were consistent with the conceptual wind-driven circulation pattern in winter but opposite in summer. Process-oriented experiments suggest that the summertime cyclonic circulation in the northern Gulf of Tonkin forms as a result of the combination of stratified wind-driven circulation and tidal-rectified inflow from Qiongzhou Strait. The interaction between the southwest monsoon and buoyancy-driven flow from Hong River can significantly intensify the cyclonic circulation near the surface, but its contribution to the vertically averaged flow of the cyclonic circulation is limited.

1. Introduction

[2] The Gulf of Tonkin is a shallow marginal sea located in the northwestern South China Sea (SCS) (Figure 1). The isobaths in the Gulf run approximately along the coast, with depths <50 m north of 19.5°N. The Gulf is connected to the northwestern shelf of the SCS on the east through Qiongzhou Strait (located between Leizhou Peninsula in Guangdong and Hainan Island) and to the southern SCS basin between Hainan Island on the east and Vietnam's coast on the west. In addition to water exchanges through these two openings, water in the Gulf is supplied by freshwater discharge from rivers that terminate along the northern coast. The Hong River is the largest river, with its mouth located near the China-Vietnam boundary around 21°N. Due to the East-Asian monsoon climate, the runoff of this river is generally larger in summer and lower in winter, with a maximum discharge rate of $>1.0 \times 10^4$ m^3 s^{-1} in August [*Chen et al.*, 2012a,b]. This rate is about 10 times larger than the sum of runoff rates from all smaller rivers entering the Gulf along the Guangxi coast (Figure 2).

[3] The water movement in the Gulf of Tonkin is driven by tides, monsoon surface forcing, and river discharge [*Wyrtki*, 1961; *Guan and Chen*, 1961; *Fang*, 1986; *Shi et al.*, 2002; *Chen et al.*, 2012a,b]. Water level recorded at tidal gauges, by satellite altimeters, and numerical model simulations indicate that the tides in this coastal region are characterized by progressive surface gravity waves dominant at the diurnal (K_1 and O_1) and semidiurnal (M_2 and S_2) frequencies [*Fang*, 1986; *Hu et al.*, 2001; *Shi et al.*, 2002]. As a result of larger diurnal tidal energy flux entering the Gulf along the western coast of Hainan, the maximum amplitude of diurnal tidal elevation in this region is about 0.5 m higher compared to that of the semidiurnal

[1]Physical Oceanography Laboratory, Ocean University of China, Qingdao, China.
[2]School for Marine Science and Technology, University of Massachusetts-Dartmouth, New Bedford, Massachusetts, USA.
[3]International Center for Marine Studies, Shanghai Ocean University, Shanghai, China.
[4]Department of Physical Oceanography, Woods Hole Oceanographic Institution, Woods Hole, Massachusetts, USA.
[5]School of Marine Sciences, Sun Yat-Sen University, Guangzhou, China.
[6]South China Sea Marine Engineering Survey Center, State Ocean Administration, Guangzhou, China.
[7]Department of Civil Engineering, Water Resource University, Hanoi, Vietnam.

Corresponding author: Y. Ding, School for Marine Science and Technology, University of Massachusetts-Dartmouth, 706 S Rodney French Blvd., New Bedford, MA 02744, USA. (yding@umassd.edu)
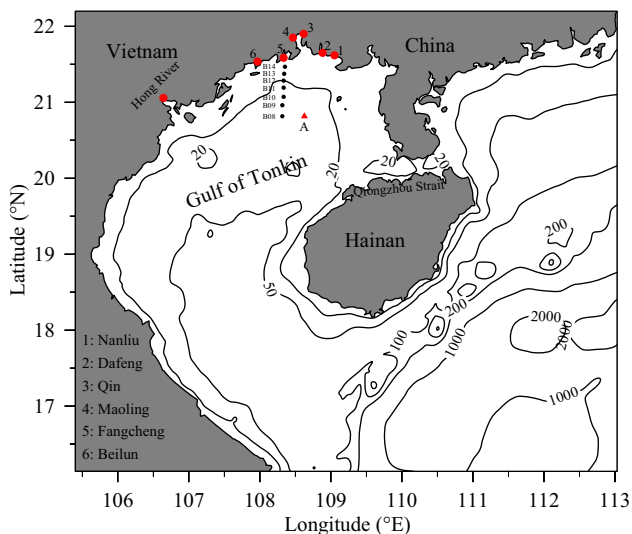
Figure 1. Map of the Gulf of Tonkin. Contours indicate isobaths in meters. Red dots are locations of the rivers. The red triangle and label "A" shows the location of the mooring site for the 1988–1989 current measurements. Black dots with labels from B08 to B14 are the hydrographic stations taken in the winter and summer seasons in 2006.


Figure 2. Climatological monthly mean freshwater discharges from the Hong River, Vietnam and rivers along the coast of Guangxi Province, China. Data for the Hong River was from *Chen et al.* [2012].

tidal elevation [*Fang et al.*, 1999]. Tidal rectification, due to the nonlinear interaction between tidal currents, bottom topography, bottom friction, and the earth's rotation, is generally weak in the interior of the Gulf but stronger near the coast, around islands and within Qiongzhou Strait [*Shi et al.*, 2002; *Chen et al.*, 2012a,b]. It is a key physical mechanism generating a net inflow into the Gulf of Tonkin through Qiongzhou Strait [*Shi et al.*, 2002].

[4] The Gulf of Tonkin is within the East-Asian monsoon regime with northeasterly (blowing from the northeast) wind during September through April and southwesterly wind during summer [*Manh and Yanagi*, 2000]. If driven purely by the monsoon wind under homogenous ocean conditions, the circulation in this region should be cyclonic in winter and anticyclonic in summer (Figure 3) [*Wyrtki*, 1961; *Guan and Chen*, 1961; *He*, 1987; *Manh and Yanagi*, 2000; *Sun and Huang*, 2001]. The cyclonic circulation in winter has been demonstrated in previous observations [*Wyrtki*, 1961; *Xu et al.*, 1980; *Zhuang et al.*, 1981]. Whether or not an anticyclonic circulation dominates in summer, however, has been recently challenged [*Shi et al.*, 2002; *Yang et al.*, 2003; *Bao et al.*, 2005; *Wu et al.*, 2008]. *Shi et al.* [2002] analyzed a 37 year current data set measured in Qiongzhou Strait and found that during summer the strait featured a relatively permanent westward flow with a net transport of ∼0.4 Sv entering the Gulf of Tonkin. Mainly tidal rectification rather than wind forcing drives this transport. This westward flow was also observed in drifter measurement reported in *Yang et al.* [2003]. These observations are contrary to the anticyclone circulation derived with wind-driven theory. *Shi et al.* [2002] believed that as an adjustment of the flow to the earth's rotation, this net westward transport could cause the water in the northern Gulf of Tonkin to move cyclonically. Motivated by the observational evidence, *Wu et al.*
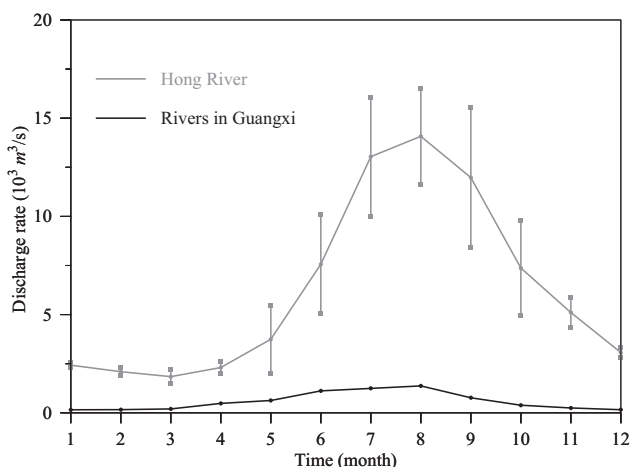
[2008] applied a potential vorticity model to investigate the physical mechanism driving the summertime circulation in the Gulf of Tonkin under homogenous conditions. Specifying the vorticity flux at the boundary connected to Qiongzhou Strait, they found that a gulf-wide cyclonic circulation could form as the potential vorticity balance in the Gulf of Tonkin in summer.

[5] No studies, to our knowledge, have considered the contribution of river discharge to the summertime circulation in the Gulf of Tonkin. Most previous modeling studies in this region were built on homogenous conditions with no buoyancy forcing. The freshwater discharge from the Hong River has a summertime average value of ∼1.0×10^4 m³ s⁻¹, with a peak greater than 4.0×10^4 m³ s⁻¹ during some wet years [*Chen et al.*, 2012a, 2012b]. In general, the river-discharge water turns anticyclonic and flows southward along the coast after it enters the Gulf of Tonkin. Since the bathymetry in the northern region is relatively flat, the river plume water could turn cyclonically northward under a southwesterly wind condition during summer. Recent hydrographic surveys [*Sun et al.*, 2009] in the northern Gulf of Tonkin showed that the water was vertically well mixed during winter, but was stratified with a significant vertical gradient above the bottom boundary layer in a region shallower than the 40 m isobath, where a small amount of freshwater discharge from local rivers along the Guangxi coast existed (Figure 4). Does the summertime circulation in this region feature an anticyclonic circulation or cyclonic circulation? If it is cyclonic, what is the key physical driving mechanism? At what level does freshwater discharge from the Hong River and stratification influence the summertime circulation in the Gulf of Tonkin? Are the tides a negligible factor for the generation of the cyclonic circulation? To our knowledge, these questions have not been addressed in previous studies.

[6] In this paper, we attempt to address these questions by analyzing direct current measurement data taken in the northern Gulf of Tonkin during 1988–1989 and process-oriented numerical modeling experiments. Due to territorial restrictions, very few direct current measurements have
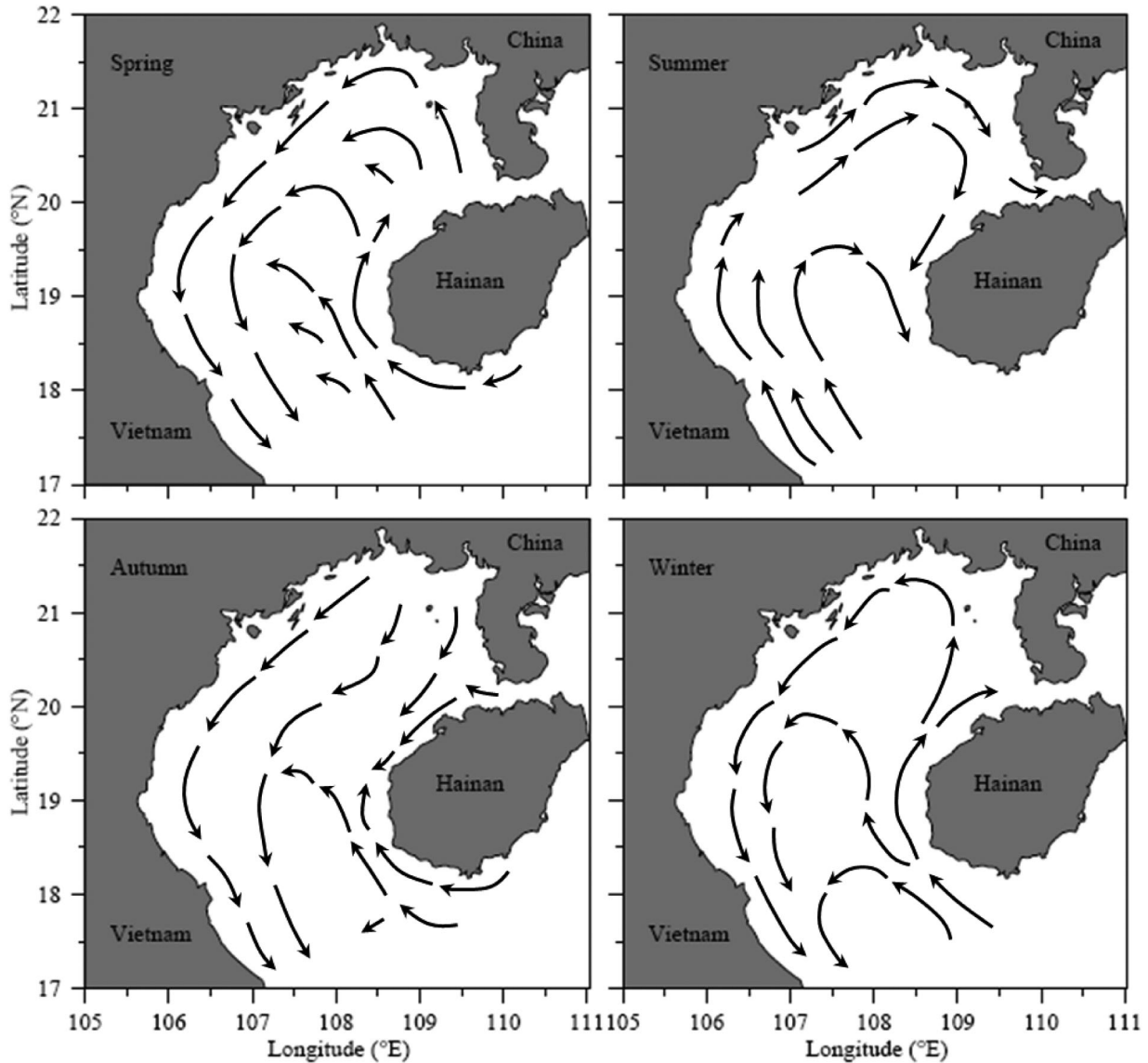
Figure 3. Schematic of the conceptual seasonal circulation patterns in the Gulf of Tonkin based on wind-driven circulation theory with consideration of the 1960s China and Vietnam joint hydrographic survey results.

been made in this region. Harmonic, spectral, low-pass filter, and correlation analyses were performed on these data with an aim at understanding the characteristics and variability of tidal and subtidal flow fields and their relationship to seasonal change in stratification and wind. Good agreement between the model-computed and observed currents at measurement sites promoted process-oriented modeling experiments for the purpose of studying the physical mechanism for the summertime circulation in the Gulf of Tonkin.

[7] The rest of the paper is organized as follows. In section 2, the current data and model used in the study are briefly described. In section 3, harmonic, spectral, and correlation analysis results of the current data are presented. In section 4, the model-data comparisons are made and process-oriented numerical experiments are carried out to study the physical mechanism for the summertime cyclonic

circulation in the northern Gulf of Tonkin. In section 5, the summary is given.

2. Field Data and Model

2.1. Current Meter Data

[8] Current measurements were made at mooring site A (shown in Figure 1) during October 1988 to September 1989 (Figure 5). Site A was located at 108°37′38″E, 20°48−49″N in the northern Gulf of Tonkin around the 40 m isobath. Aanderaa-type (Recording Current Meter (RCM8)) current meters were deployed at depths of 10, 20, and 30 m below the surface. During this deployment, the wind was recorded hourly at site A. For a variety of reasons, some current records have data gaps over the measurement period. The longest gap was 43 days in the 20 m record during March to April, 1989. The analysis was
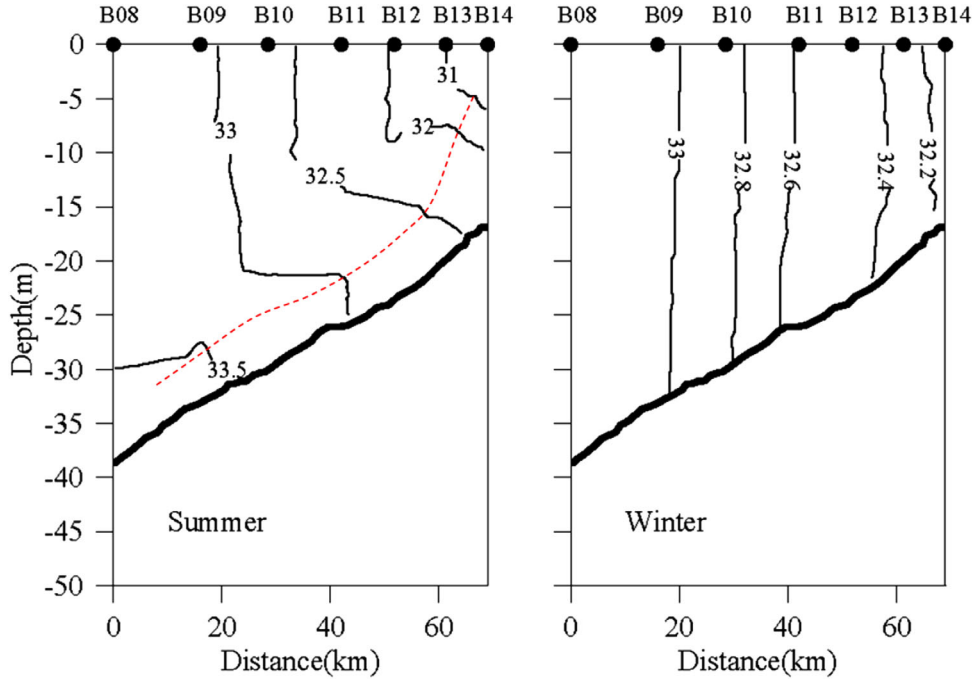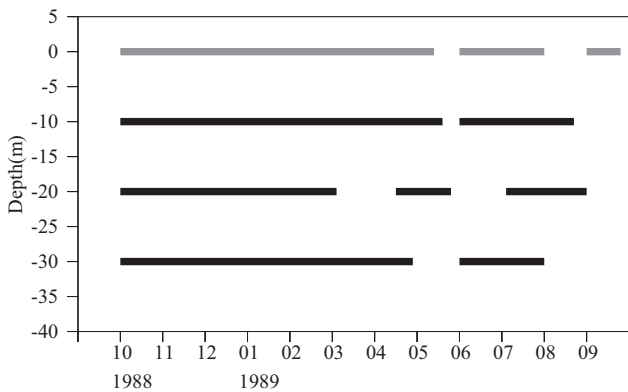
Figure 4. Summertime and wintertime salinity distributions on transect B08-B14 in the northern Gulf of Tonkin measured during hydrographic surveys made in summer and winter, 2006. Red dashed line denotes the height of the bottom boundary layer in the summer season. The salinity data were digitalized from figures listed in *Sun et al*. [2009].

conducted using the hourly sampled data. A 3 h low-pass filter was applied to convert 0.5 h sampled data to hourly records. Rotary spectra for the water velocity were calculated to identify the prominent energy signals and frequencies. Harmonic analysis and the band-pass filtered complex demodulation method were used to examine the characteristics and variability of barotropic and internal tidal currents at the site. The subtidal flow is defined as the 33 h low-passed filtered velocity. Correlation analysis was performed between subtidal currents and wind velocity to qualify the role of wind forcing in the seasonal variability of the circulation in the Gulf of Tonkin.

Figure 5. Time line of the 1988–1989 measurements at site A. Black heavy lines: water current measurements. Gray heavy line: wind measurements.

2.2. The Model

[9] We compared the observed water velocity to the model-computed velocity at site A. The model used for this comparison was the Global-FVCOM developed recently by the joint research team of University of Massachusetts-Dartmouth (UMASSD) and Woods Hole Oceanographic Institution (WHOI). Global-FVCOM was built under the platform of the unstructured-grid Finite-Volume Community Ocean Model (FVCOM) [*Chen et al*., 2003, 2006a, 2006b, 2012a, 2012b]. It is a fully ice-ocean coupled primitive equation unstructured-grid, finite-volume ocean model that is driven by (a) astronomical tidal forcing with eight constituents (M_2, S_2, N_2, K_2, K_1, P_1, O_1, and Q_1), (b) surface wind stress, (c) net heat flux at the surface plus short-wave irradiance in the water column, (d) surface air pressure gradients, (e) precipitation (P) minus evaporation (E), and (f) river discharge [*Gao et al*., 2011]. The model features a horizontal resolution of $\sim$2–5 km (measured by the length of the longest edge of a triangular cell) within the Arctic and US coastal regions and of $\sim$15 km in the Gulf of Tonkin, SCS. The vertical grid is constructed with a hybrid terrain-following coordinate with a total of 45 layers [*Chen et al*., 2009]. The s coordinate was used in regions with depth greater than 225 m, with 10 uniform layers (5 m thick) near the surface and five uniform layers (5 m thick) near the bottom, respectively, to better resolve surface and bottom boundary layers. In shelf and coastal regions of depth less than 225 m, the σ coordinate with a uniform layer thickness is specified. The coordinate transition thus occurs smoothly at a depth of 225 m where all layers have a uniform thickness of 5 m. In the Gulf of

4

Tonkin, the vertical solution is 2.2 m or less in the regions shallower than 100 m. Global-FVCOM is integrated numerically with time using a semi-implicit FVCOM solver with a default setup of the modified Mellor and Yamada level 2.5 (MY-2.5) and Smagorinsky turbulent closure schemes for vertical and horizontal mixing, respectively [*Mellor and Yamada*, 1982; *Smagorinsky*, 1963]. The time step used for integration was 300 s.

[10] With a 50 year spin-up, Global-FVCOM has been run under realistic forcing conditions for the 35 year period 1978–2012. The model results were and are being validated in the Arctic, northwest Atlantic Ocean shelf regions, and other regions [e.g., *Chen et al.*, 2009; *Gao et al.*, 2011; *Chen et al.*, 2012a, 2012b; *Hu et al.*, 2012; *Lai et al.*, 2013]. To identify and quantify the physical driving mechanism for the summertime circulation in the Gulf of Tonkin, we reran Global-FVCOM for 1988–1989 by turning off or on stratification, tides, Hong River discharge, winds, and surface heat flux. It was approached by running a subdomain Gulf of Tonkin FVCOM that was constructed using the same grid of Global-FVCOM and nesting with Global-FVCOM outside the SCS. With the same grids used in both subdomain and global models, running the subdomain model shows the same results in the Gulf of Tonkin as running the Global-FVCOM. This approach enabled us to conduct the process-oriented experiments efficiently.

3. Results From Current Measurements

3.1. Structure of Barotropic and Internal Tidal Currents

[11] Rotary spectral analysis [*Gonella*, 1972; *Chen et al.*, 1996] was performed on the site A hourly current time series. Distributions of the rotary spectra energy with respect to frequency were similar at the measurements depths throughout the water column (Figure 6); all featured two prominent peaks at the diurnal and semidiurnal frequencies. Both the clockwise-rotating and counterclockwise-rotating motions were significant for diurnal and semidiurnal tidal currents. The clockwise-rotating component was slightly higher than the counterclockwise-rotating component, suggesting that the sum of these two components exhibited clockwise rotation. The total energy was higher for diurnal than for semidiurnal tidal currents, which is consistent with previous measurements of tidal elevation in the Gulf of Tonkin [*Fang et al.*, 1999]. At site A, the tidal energies were slightly higher at a depth of 20 m than at depths of 10 and 30 m. The current measurements covered the summer season during 1988–1989, suggesting that the vertical profile of tidal currents could differ due to the seasonal change in water stratification.

[12] The local inertial period in the Gulf of Tonkin is ~33.7 h (1.4 days), which corresponds to a frequency of 0.712 cpd. No significant peak was found at or near the inertial frequency in the 1988–1989 currents records (Figure 6), implying that inertial oscillations were insignificant in the northern Gulf of Tonkin

[13] Using the T_TIDE harmonic analysis program [*Pawlowicz et al.*, 2002], we calculated the tidal ellipse parameters of the four dominant tidal constituents (O_1 and K_1 for diurnal tides; M_2 and S_2 for semidiurnal tides). Analysis was performed at all measurement depths for each
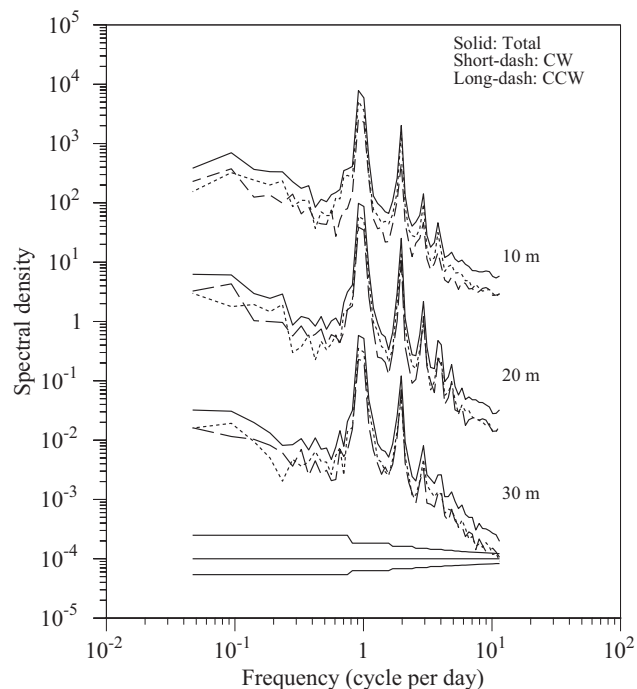

Figure 6. Rotary spectra of water velocities measured at depths of 10, 20, and 30 m during the 1988–1989 deployment. Total: the total energy. CW: the clockwise energy. CCW: the counterclockwise energy. The spectra at the depth of 20 m are shifted downward by 10^2, and spectra at the depth of 30 m are shifted downward by 10^4. Rotary spectra were estimated using the hourly data. Spectra density is in $(cm/s)^2/cpd$.

season. The results (Figure 7 and Table 1) clearly show that in general diurnal tidal currents were stronger than semidiurnal tidal currents, and both of them were stronger during summer than during winter. For example, at 20 m, the O_1, K_1, and M_2 tidal ellipse major axes were 10.2, 10.7, and 7.3 cm s^{-1} in winter, but reached 13.2, 11.9, and 11.2 cm s^{-1} in summer, accounting for a seasonal difference of ~3 cm s^{-1} for diurnal tidal currents and ~4.6 cm s^{-1} for semidiurnal tidal currents. This difference is likely due to seasonal changes in stratification, since the water was vertically well mixed during winter but stratified during summer.

[14] The seasonal difference in tidal amplitudes can be viewed more clearly in the frequency band-passed complex demodulation analysis shown in Figure 8. The bandwidth was 0.82–1.19 cpd for diurnal tidal constituents and 1.69–2.25 cpd for semidiurnal tidal constituents. Both diurnal and semidiurnal tidal currents exhibited a significant fortnightly variation due to the spring and neap tidal cycles. The current difference between neap and spring tides was roughly ~6–10 cm s^{-1}. In addition to the fortnightly variation, the tidal current amplitudes at all measurement depths were significantly higher during summer. The maximum seasonal difference at the spring tide was ~3 cm s^{-1}, which accounted for a difference of ~30% of the spring tidal current measured during winter.

[15] The tidal intensification during summer was consistent with the seasonal change of water stratification. During
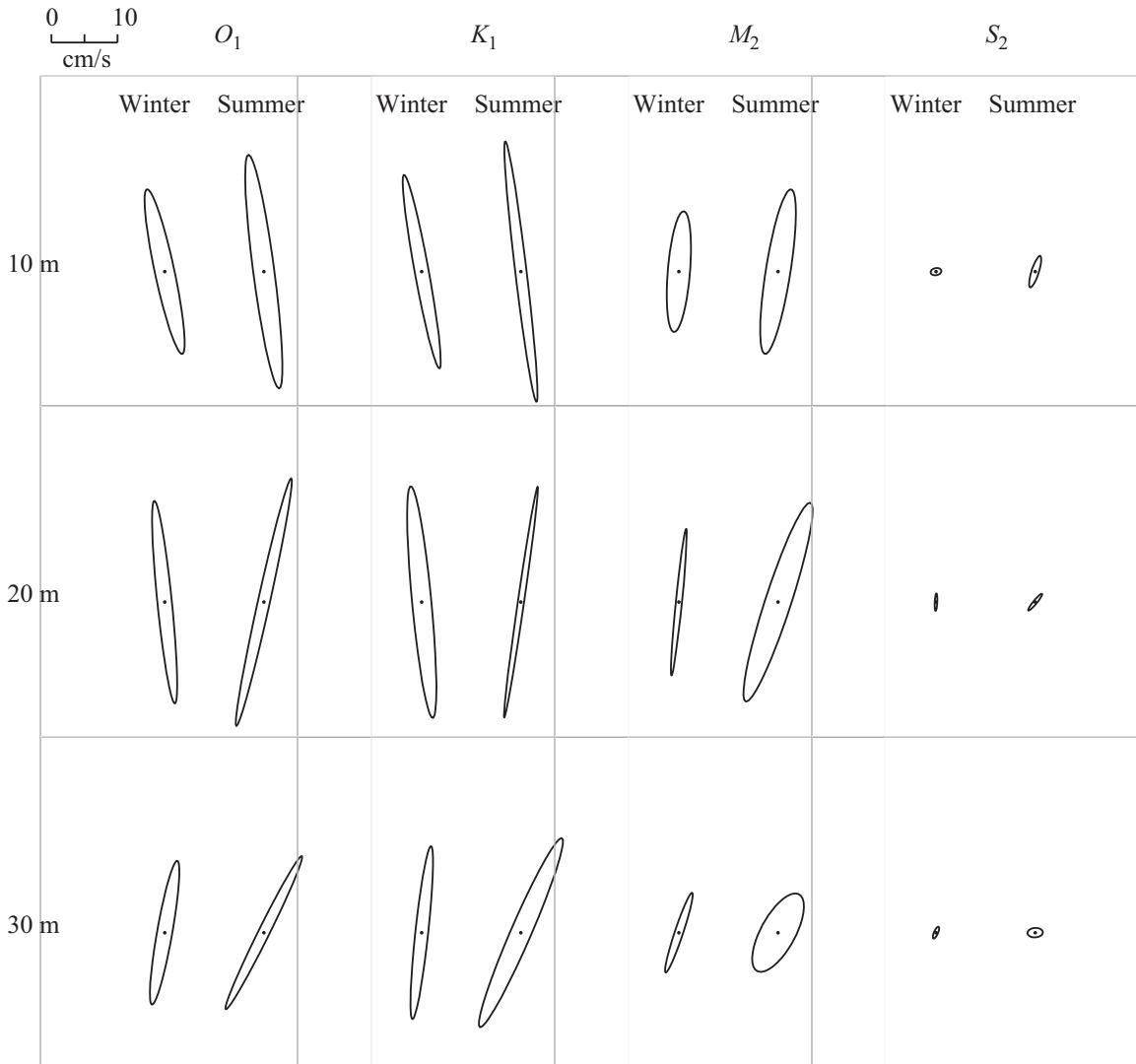
Figure 7. Tidal current ellipses for O_1, K_1, M_2, and S_2 constituents at depths of 10, 20, and 30 m at site A for the winter and summer periods of 1988–1989.

1988–1989, satellite-derived sea surface temperature (from the NOAA High-resolution Blended Analysis of Daily SST: http://www.esrl.noaa.gov/psd/data/gridded/data.noaa. oisst.v2.highres.html) at the measurement site clearly shows a significant seasonal variability; from 20°C in January to 28–29°C during June through September (Figure 9: top). Correspondingly, the Global-FVCOM-computed water temperature and salinity were vertically well mixed during January through May, while the water was stratified during June through September (Figure 9: middle and bottom). The summertime stratification was not only driven by the seasonal change in surface heat flux but also by an increase of freshwater discharge from local rivers. These features were consistent with the recent hydrographic observations shown in Figure 4.

[16] The observed seasonal variability of tidal currents and water stratification indicate that the seasonal difference in tidal current amplitudes can be attributed to the occurrence and intensification of internal tides during summer. It suggests that the internal tidal currents during summer

could account for ~30% of the total tidal energy, a considerable amount that could not be ignored. It is well known that internal tides are energetic in the SCS, especially in the slope regions and around islands [*Yuan et al.*, 1995; *Zhang and Jiang*, 1999; *Liang et al.*, 2005; *Chen et al.*, 2007]. However, there have been few studies aimed at internal tides in the shallow northern Gulf of Tonkin. The acoustic Doppler current profiler (ADCP) measurements made by *Chen et al.* [2007] were at the 70 m isobath near the slope in the southern Gulf of Tonkin where the water column remains stratified throughout the year.

3.2. Subtidal Currents

[17] The subtidal currents were defined here as the 33 h low-pass filtered water velocity. The low-pass PL64 filter [*Beardsley and Rosenfeld*, 1983] was used and the filtered data resampled at a 6 h interval. The same filter was also applied to construct the low-frequency wind velocity. During October 1988 through February 1989, the northeast monsoon prevailed at site A (Figure 10). Except in

Table 1. Tidal Current Ellipse Parameters at Different Measurement Depths for Winter (W) and Summer (S)[a]

Constituents	Frequency (h^{-1})	Layer (m)	Major/(cm/s) Error/(cm/s)		Minor/(cm/s) Error/(cm/s)		Inclination/° Error/°		Phase/° Error/°	
			W	S	W	S	W	S	W	S
O$_1$	0.03873	10	8.7	12.0	−1.3	−1.6	108.3	101.3	207.4	207.5
			1.0	1.7	0.8	1.1	5.7	5.7	7.6	8.6
		20	10.2	13.2	−1.1	−0.9	97.0	71.6	205.7	220.5
			1.1	2.7	0.4	2.6	2.8	11.6	6.7	11.5
		30	7.8	9.6	−0.8	−0.8	76.5	53.2	207.1	197.6
			0.7	2.6	0.4	2.4	6.8	13.0	7.5	16.8
K$_1$	0.04178	10	8.5	13.4	−0.7	−0.8	106.6	100.2	264.3	264.6
			1.0	1.6	0.8	1.2	6.4	5.2	7.2	8.3
		20	10.7	11.9	−1.1	0.5	97.3	77.7	259.2	278.9
			1.1	2.5	0.5	2.5	2.4	14.7	6.3	14.5
		30	8.2	11.4	−1.2	1.4	80.1	56.7	261.4	266.2
			0.8	3.0	0.8	2.2	6.1	13.1	5.5	18.3
M$_2$	0.08051	10	5.9	8.5	−1.8	−1.8	81.9	76.3	214.2	227.5
			0.5	1.1	0.5	0.5	6.0	4.3	7.2	8.3
		20	7.3	11.2	−0.3	−1.9	81.8	63.6	200.9	213.6
			0.7	1.4	0.4	1.6	4.2	8.8	6.0	7.8
		30	4.8	5.1	0.8	−2.3	69.0	45.5	202.8	224.1
			0.7	1.3	0.5	1.5	8.6	26.2	10.7	21.2
S$_2$	0.08333	10	1.3	1.8	−1.1	−0.5	77.2	63.1	273.0	288.5
			0.5	1.0	0.4	0.7	25.1	26.0	92.0	36.0
		20	2.1	1.3	−0.7	−0.2	80.0	38.4	246.4	11.1
			0.6	1.3	0.4	1.1	20.0	12.0	30.0	10.2
		30	1.3	1.2	0.1	0.5	73.1	1.9	289.9	328.3
			0.7	1.2	0.6	1.0	31.0	20.0	34.0	94.6

[a]The sign of the minor axis of the tidal current ellipses indicates the direction of rotation: negative for clockwise rotating and positive for counterclockwise rotating. Inclination is measured counterclockwise from East. Phase is given with respect to Greenwich. The term "Error" indicates the 95% uncertainty estimate computed by T_Tide.

December 1988, the northeasterly wind was relatively stable in direction and its speed varied in the range of 5–15 m s^{-1}. Correspondingly, the upper ocean layer was dominated by the northwestward flow with speeds of 5–14 cm s^{-1}. The water velocity showed a clockwise rotation with water depth, illustrating the nature of the wind-driven flow near the surface and Ekman spiral in the vertical (Figure 10). This flow structure is consistent with the cyclonic circulation proposed based on wind-driven theory in previous studies [*Wyrtki*, 1961]. During March to May 1989, the wind velocity varied with a time scale of 5–7 days and wind speed was significantly weaker than the previous winter. In March, the water velocity at a depth of 10 m was dominated by a northwestward or westward flow in March, while during April through May the 10 m current varied significantly and was often opposite to the wind direction (Figure 10). The water velocity appeared to be more variable with no preferred direction during summer from June to August 1989. The relatively strong southwest monsoon prevailed in June, but at a depth of 10 m, the southeastward flow only existed for a few days and predominately westward or southwestward flow persisted during the rest of the month. In late July and early August, the near-surface flow was sometimes in the same direction as the wind. It is clear that during winter and even late spring, the observed flow direction at site A was not consistent with the direction of an anticyclonic circulation as derived by wind-driven theory [*Wyrtki*, 1961].

[18] The 10 m current measurements at site A showed that the northwestward flow predominated during both winter and summer seasons. This suggests that during these two seasons, the flow in the northern Gulf of Tonkin featured a cyclonic circulation. We calculated the correlation between the 33 h low-pass filtered wind and current velocities for each season in 1988–1989. Figure 11 shows the correlation map of the 10 m northwestward current component with the wind velocity at a 10 m height over the direction range of −180° to 180° for the winter and summer seasons. The data showed that the northwestward current was dominant during the measurement period, so that the analysis was done by projecting current vectors to the northwest direction. This analysis was done with consideration of the significant confidence level, resulting in a critical value of 0.31 at 99% confidence level and of 0.22 at 95% confidence. During the winter season, the near-surface water current was clearly correlated with the wind velocity. The highest correlation coefficient of ∼0.8 was found in a direction range of 40°–75°. Since the direction of the northeast monsoon did not change much during winter, the wind-current correlation showed almost no difference at different lags. During the summer season, however, the correlation coefficient between near-surface water current and wind were about ∼0.5 or lower. The direction between the water and wind velocities at the maximum correlation coefficient decreased as the time lag became longer. This result suggested that although the correlation coefficient in
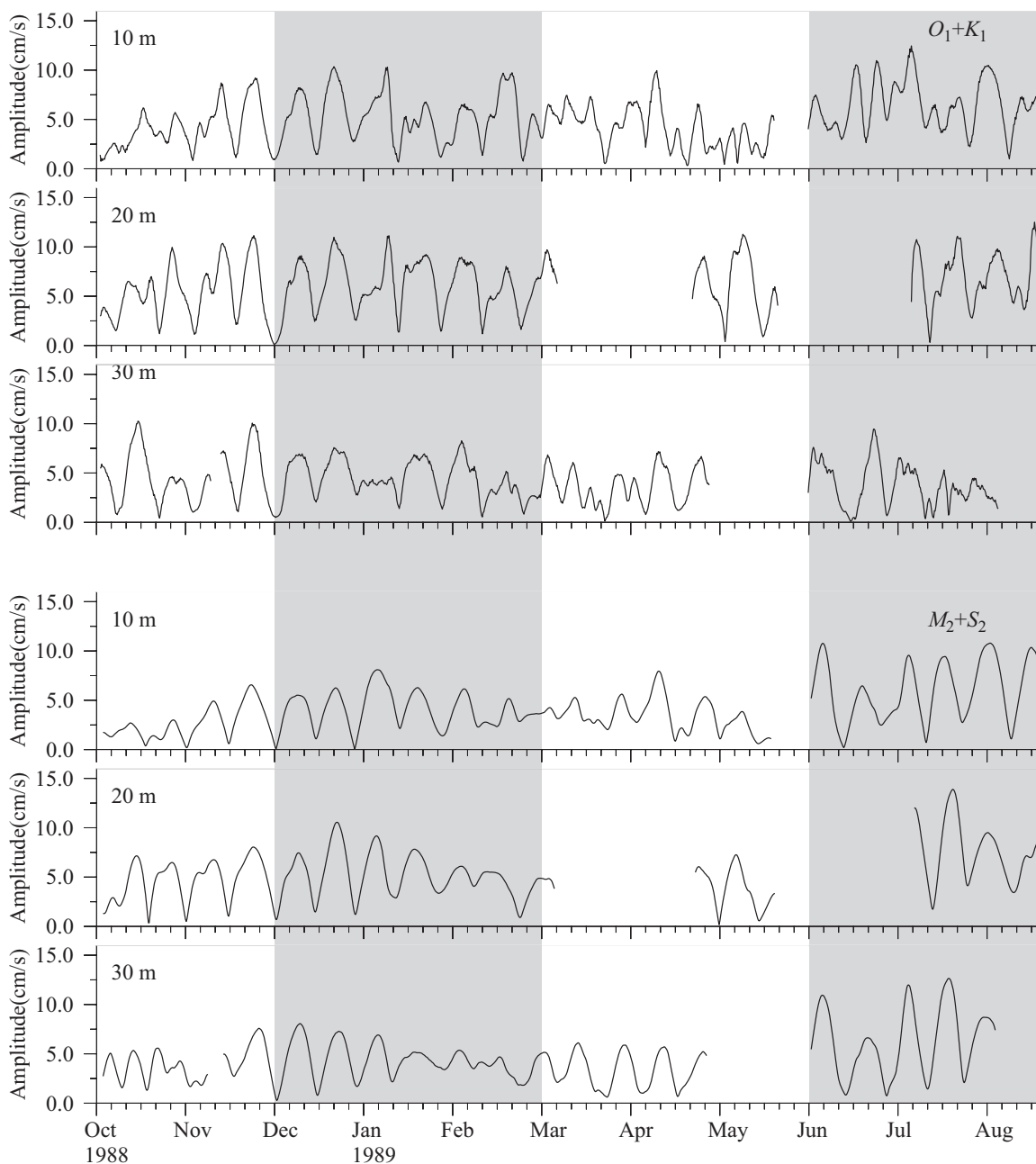
Figure 8. Time series of amplitudes of diurnal and semidiurnal tidal currents calculated using band-passed complex demodulation at depths of 10, 20, and 30 m from October 1988 to August 1989.

summer was still higher than the critical level, the wind would not be a predominant forcing to drive the summer-time circulation in the Gulf of Tonkin.

4. Process-Oriented Studies of the Summertime Circulation

[19] The freshwater discharge from the Hong River and wind fields during 1988 and 1989 exhibited significant interannual variability (Figure 12). In 1988, the river runoff showed two peaks with a discharge rate greater than $\sim 1.7 \times 10^4$ m^3 s^{-1} in July and September, respectively, while in 1989, the river runoff featured three peaks in June, July,

and October, with a maximum discharge rate greater than of $\sim 2.1 \times 10^4$ m^3 s^{-1} around mid June. The southwest monsoon prevailed during the summer seasons of 1988 and 1989, but the wind speed was much stronger in 1988 than 1989. We have used Global-FVCOM to examine the physical mechanisms that drive the summertime circulation in the northern Gulf of Tonkin, with a focus on the contributions of stratification, inflows from the Hong River and Qiongzhou Strait, and wind forcing. This study was approached by two steps: (1) validating the model through comparison with the current measurements taken in 1988–1989, and (2) using the validated model to carry out process-oriented experiments to quantify the contributions
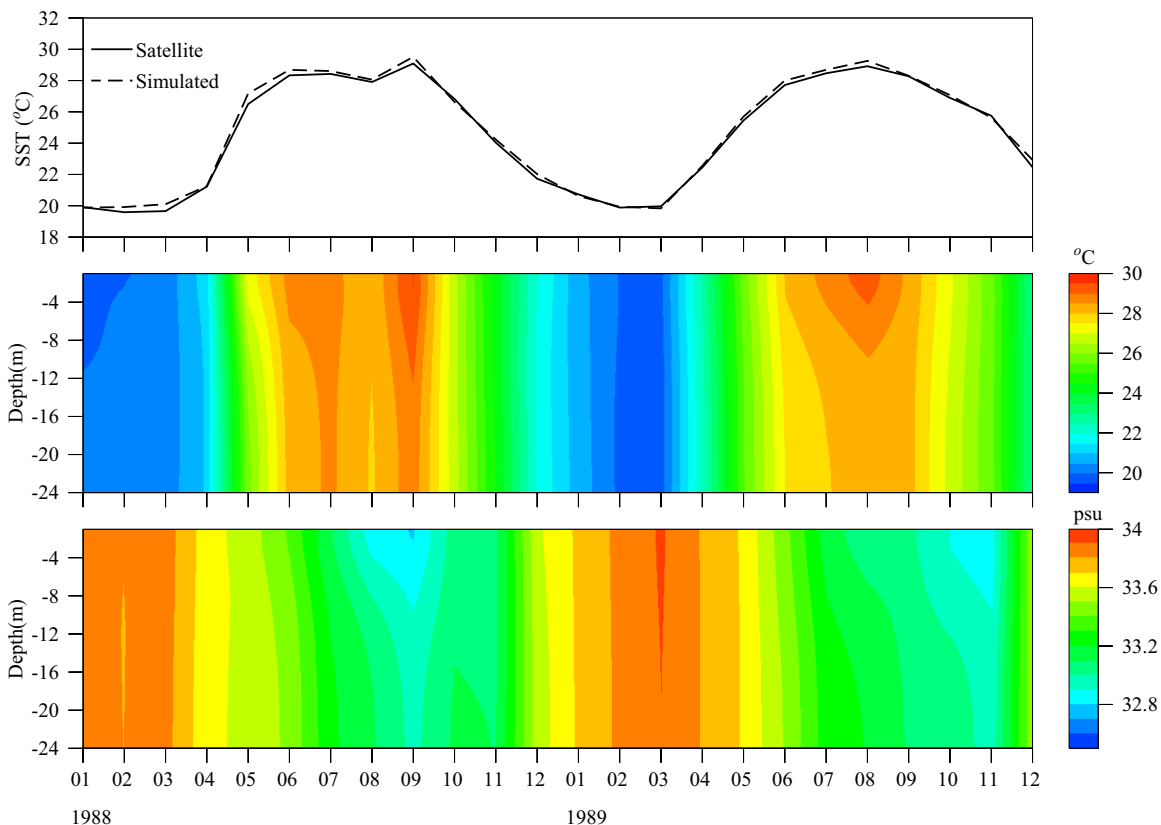
Figure 9. Time series of (top) the satellite-derived sea surface temperature (SST) and (middle) the Global-FVCOM-calculated temperature and (bottom) salinity at site A from January 1988 to December 1989.

of different forcing to the formation of the summertime circulation in the region. Results of these two efforts are summarized as follows.

4.1. Model-Data Comparisons

[20] We inserted the observed monthly averaged current vectors at site A into the fields of the Global-FVCOM-computed monthly averaged current vectors for the period October 1988 to August 1989. As an example, the 10 m comparison is shown in Figure 13. The model-predicted local currents around site A matched well in both amplitude and direction the observed currents in the first 10 months. To get better statistical tests, we performed a complex vector correlation analysis [*Kundu*, 1976; *Crosby et al.*, 1993]. The result showed that the observed and the model-predicted local currents around site A were well correlated and reasonably matched in amplitude and direction (see bottom right plot in Figure 13 and Table 2). The mean observed and modeled currents were 3.6 cm s^{-1} toward 282°N and 4.5 cm s^{-1} toward 282°N, and the mean observed and modeled speeds were 4.4 cm s^{-1} and 4.7 cm s^{-1}, respectively. The complex vector correlation coefficient between the two time series was 0.95 with the model current vector oriented 8.8° clockwise relative to the observed current vector [*Kundu*, 1976]. The vector correlation computed between these two time series was 0.95, well above the ∼0.6 value for no correlation [*Crosby et al.*,

1993]. Global-FVCOM showed computed currents in Qiongzhou Strait remained westward all months over a year, which was consistent with previous observations reported in *Shi et al.* [2002].

[21] According to the model-computed current fields, in October 1988, the entire Gulf of Tonkin exhibited cyclonic circulation. This gulf-wide cyclonic circulation consisted of two flow systems: one flowing into the southern Gulf of Tonkin along the southern and western coasts of Hainan Island, and another from the westward flow through Qiongzhou Strait. This circulation pattern remained until January 1989, but the currents gradually weakened with time. In February 1989, two relatively weak cyclonic gyres formed in the northern and southern Gulf of Tonkin, respectively, and remained there until March 1989. The northern cyclonic gyre significantly intensified in April, while the southern cyclonic gyre also became stronger as the southward flow shifted eastward. During the summer season, the circulation in the southern Gulf of Tonkin varied significantly with time, but the cyclonic gyre remained in the northern Gulf of Tonkin throughout this season.

[22] Comparing the model-computed near-surface circulation patterns (shown in Figure 13) with the conceptual circulation patterns predicted by wind-driven theory (shown in Figure 3), we note that they were similar during the winter of 1988–1989 but opposite during the summer of June to August 1989. During spring 1989, the model-

9
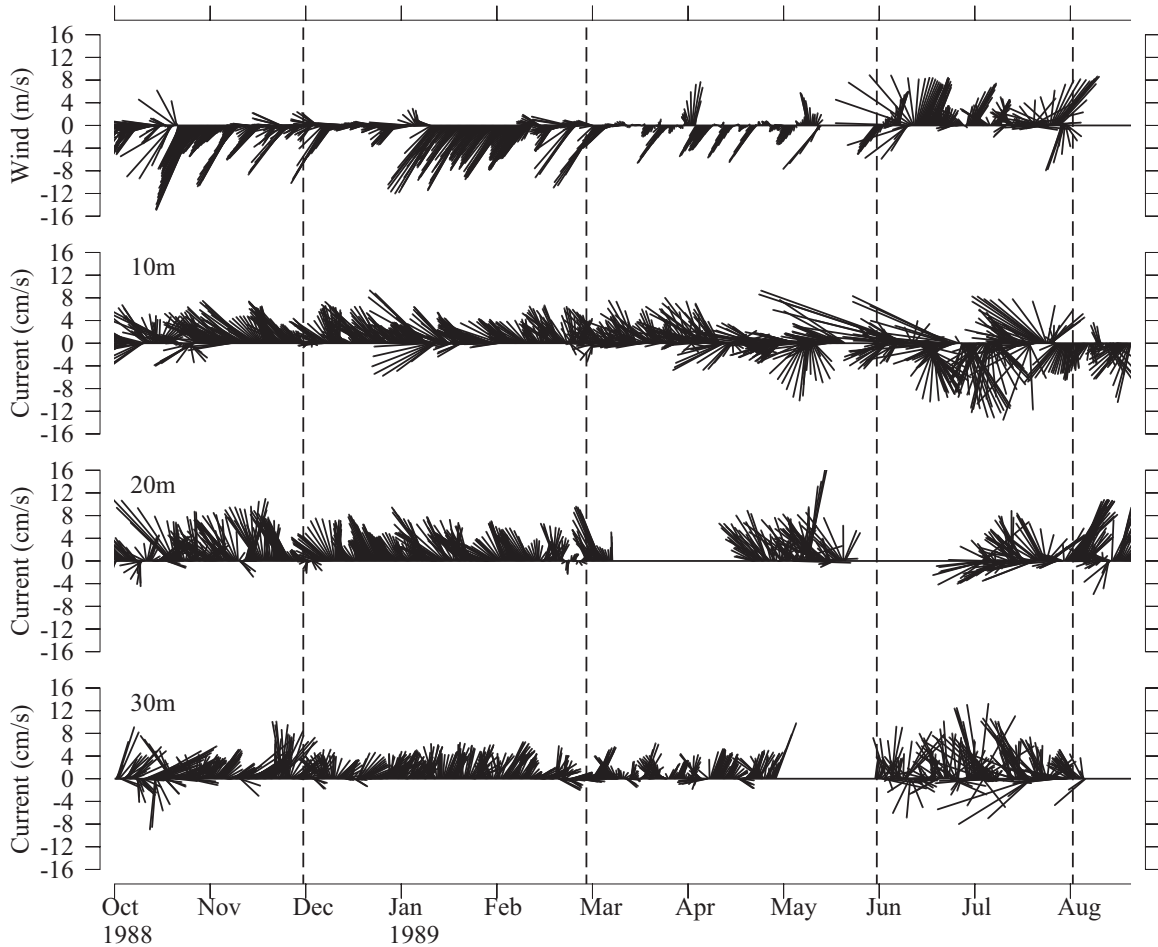
Figure 10. A 33 h low-passed filtered wind vectors at 10 m height and subtidal currents at depths of 10, 20, and 30 m for the period October 1988 to August 1989. Dashed line: the boundary defined for the seasons.

computed circulation also differed from the conceptual circulation patterns, even though both featured cyclonic circulation in general.

[23] During summer 1989, the southwest monsoon was very weak. One could argue that the disagreement between the model-computed and conceptual circulation patterns was due to weakening of the southwest monsoon during that summer. In the northern Gulf of Tonkin, however, the freshwater discharge from the Hong River was large in both summers. Considering this flow, we found that the southwest monsoon during summer could turn this buoyancy flow northward and thus intensify the cyclonic
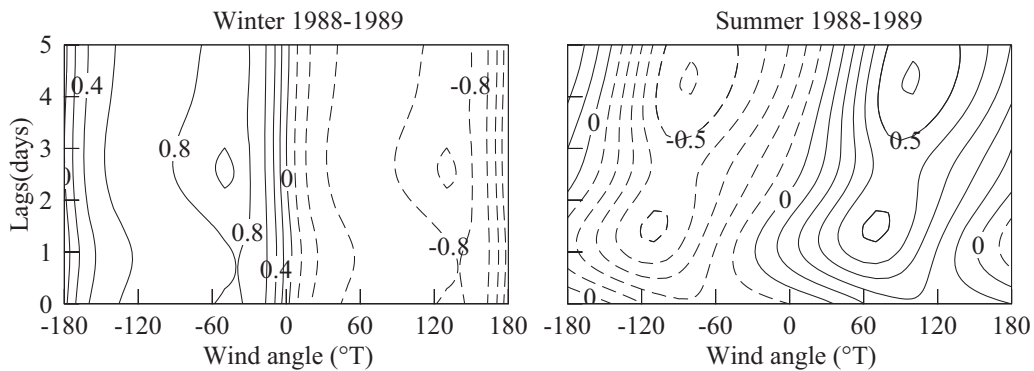
Figure 11. Correlations between observed subtidal currents at 10 m depth and surface wind velocity at 10 m height for the winter and summer seasons of 1988–1989. Analysis was done by projecting subtidal currents to the northwest direction. The critical value was 0.22 for a 95% confidence level.
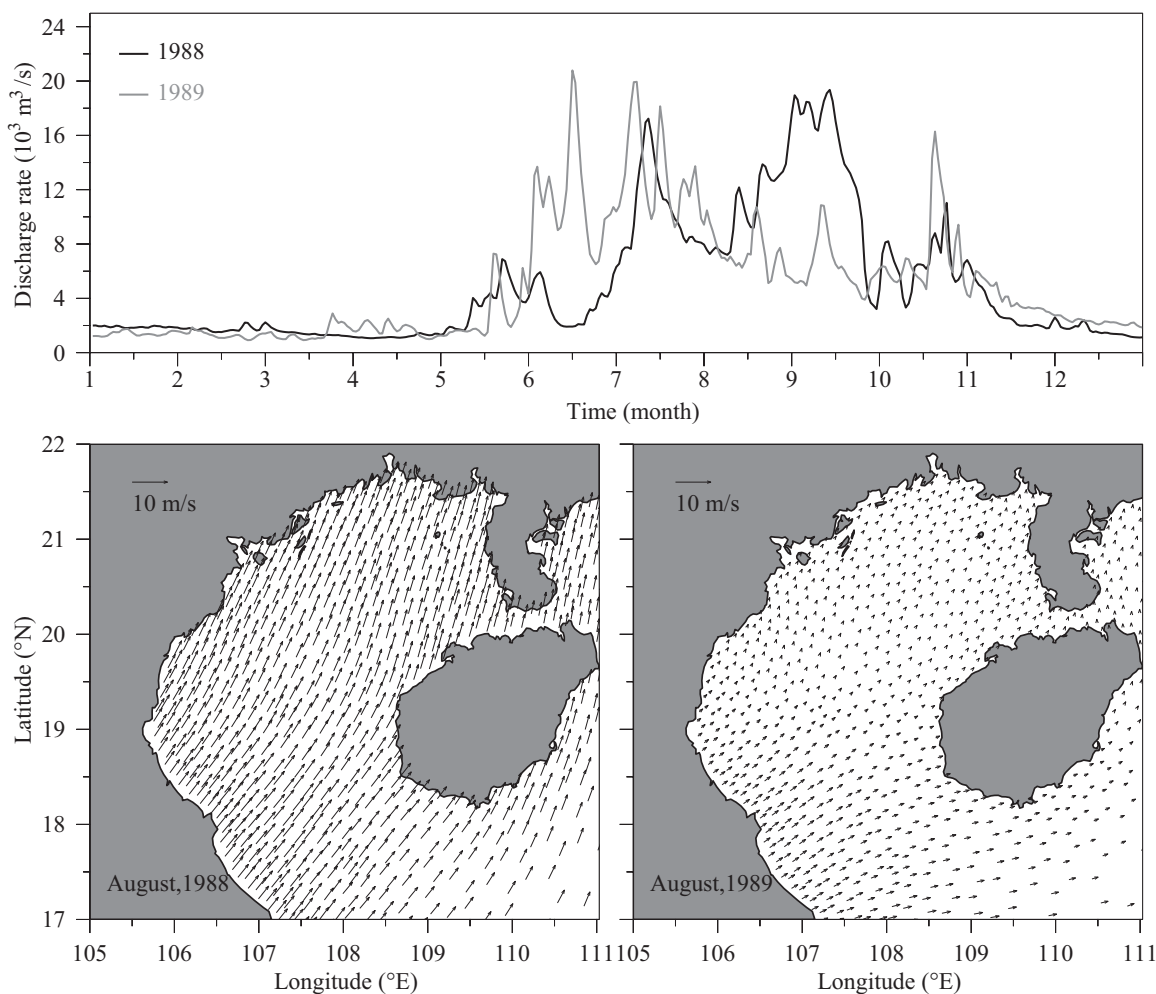
Figure 12. (top) Time series of freshwater discharge from the Hong River over 1988 and 1989, respectively, and (bottom) maps of the monthly averaged 10 m wind velocity for August of 1988 and 1989.

circulation, preventing anticyclonic circulation in the northern Gulf of Tonkin.

[24] Most of the freshwater entering the northern Gulf of Tonkin came from the Hong River during June through August in both years. As a result, in August 1988, in addition to creating a relatively strong northward flow near the western coastal region, the strong southwest monsoon also pushed the river discharge-induced low-salinity plume water offshore and then turned cyclonically in the eastern region (Figure 14). This wind-induced and buoyancy-induced cyclonic circulation appeared in a thin layer near the surface. After averaging throughout the water column, only northward flow along the western coast remained. This flow encountered and joined the cyclonic flow originating from the Qiongzhou Strait in the northern coast. In August 1989, since the southwest monsoon was very weak, the river discharge-induced low-salinity plume at the surface turned anticyclonic and moved southward along the western coast. The weak southwesterly wind did push the water over the western shelf in the northern Gulf of Tonkin offshore, but these offshore waters encountered and joined the cyclonic flow that originated from Qiongzhou Strait. In this case, the vertically averaged flow field in the

northern Gulf of Tonkin was still characterized by cyclonic flow.

4.2. Process-Oriented Experiment Results

[25] Four experiments were made to qualify the roles of wind forcing, tidal rectification, freshwater discharge and stratification in the formation of the cyclonic circulation in the northern Gulf of Tonkin during the summer season. In experiment 1 (Ex1), the model was driven by only wind forcing under homogeneous ocean conditions. In experiment 2 (Ex2), the model was driven by only tidal forcing under homogenous ocean conditions. In experiment 3 (Ex3), the model was forced by the same forcing as in Ex1 but with water stratification. In experiment 4, the model was forced by wind and tidal forcing under the same stratification condition as in Ex3. The 1988 simulation results (Figure 14) are referred to as the base case with the same forcing and stratification conditions as in Ex4 plus including river discharge. To compare the results of these process-oriented experiments with the base case, all four experiments were run at the beginning of 1988.

[26] In Ex1, the southwest monsoon generated a northward flow near the surface in the region north of 19°N,
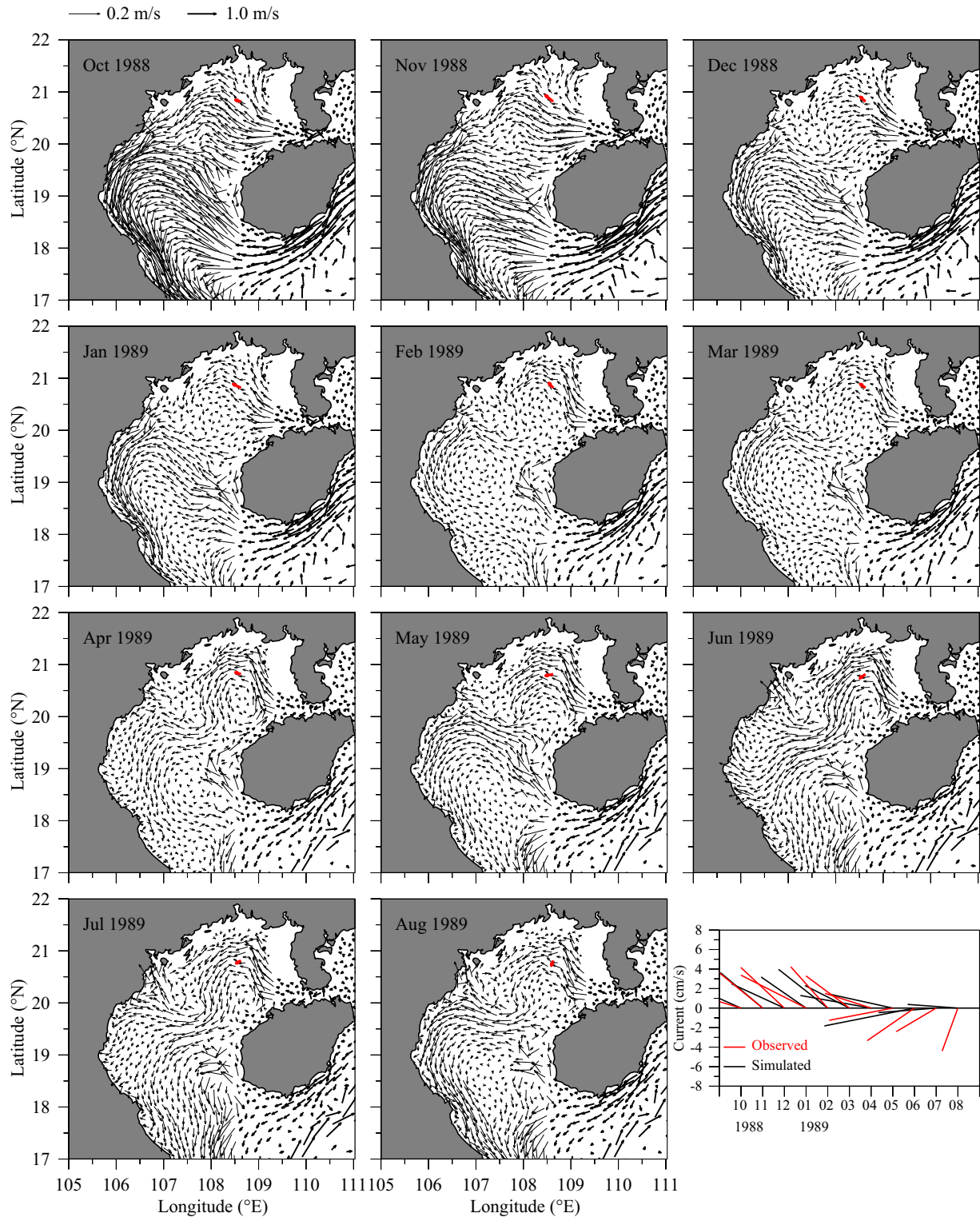
Figure 13. Maps of Global-FVCOM-computed monthly averaged current vectors at 10 m depth in the Gulf of Tonkin for the period October 1988 to August 1989. Monthly averaged current vectors observed at 10 m depth at site A are superposed in these figures (red vectors). The comparison of the 10 m model-computed and observed monthly mean vector currents at site A is shown in the bottom right plot.

which is strong in western and eastern shallow coastal regions (Figure 15). The northward flow in the eastern region separated into two branches around 20°N, one turned eastward and entered the Qiongzhou Strait, and another continuously moved northward, turned westward and encountered northward coastal flow from the western

Table 2. Statistics of the Monthly Mean Observed Current and Model-Predicted Current at 10 m at Site A[a]

	Mean	Standard	Minimum	Maximum
u	−3.6	1.1	−5.0	−1.2
v	0.8	2.5	−3.2	4.0
Sp	4.4	0.9	3.5	6.3
u_m	−4.3	1.1	−6.9	−3.2
v_m	1.3	1.3	−1.4	3.0
Sp_m	4.7	0.9	3.8	7.0

[a]All values in cm s^{-1}. The observed variables are east (u), north (v), and speed (Sp). The model variables are east (u_m), north (v_m), and speed (Sp_m).

shelf near the northern coast. In the region south of 19°N, southwesterly wind pushed the water offshore and flow toward Hainan Island, and a large portion of this water moved northeastward along the southern coast of Hainan Island. The resulting vertically averaged currents show a well-defined anticyclonic circulation in both northern and southern regions, which is the same pattern as the conceptual summertime circulation shown in Figure 3. This result demonstrates that if the Gulf of Tonkin is under homogeneous conditions and wind is the only forcing, then the circulation should be dominated by anticyclonic circulation.

[27] In Ex2, a well-defined westward flow, due to tidal rectification, was predicted in Qiongzhou Strait (Figure 16), similar to in situ measurements and model experiment results described by *Shi et al.* [2002]. *Shi et al.* [2002] clearly elaborated the tidal rectification mechanism that drives this flow. After entering the northern Gulf of Tonkin, this tidal-rectified flow turns northward and flows along the 20 m isobath. This northward flow turns westward along the 20 isobath in the northern shelf to form a cyclonic flow in the northern Gulf of Tonkin. This result indicates that even under homogenous conditions, a cyclonic circulation could form in the northern Gulf of Tonkin by inflow from tidal-rectified currents through Qiongzhou Strait.

[28] In Ex3, when stratification is added, the model run with only wind forcing produced circulation patterns similar to those from Ex1. However, the surface currents were significantly intensified (Figure 17: top leftmap). As a result, the vertically averaged cyclonic flow, which was restricted in a small region near the northern coastal region in homogenous conditions, grew in size and occupied a large area in the region north of 20.5°N (Figure 17: bottom left map). In this case, the flow entering the Qiongzhou Strait weakens, although the northward flow on the western coast remained little changed. This result suggests that even with the absence of tidal-rectified flow from Qiongzhou Strait, the cyclonic circulation in the northern Gulf of Tonkin could be driven by the southwest monsoon in stratified conditions.
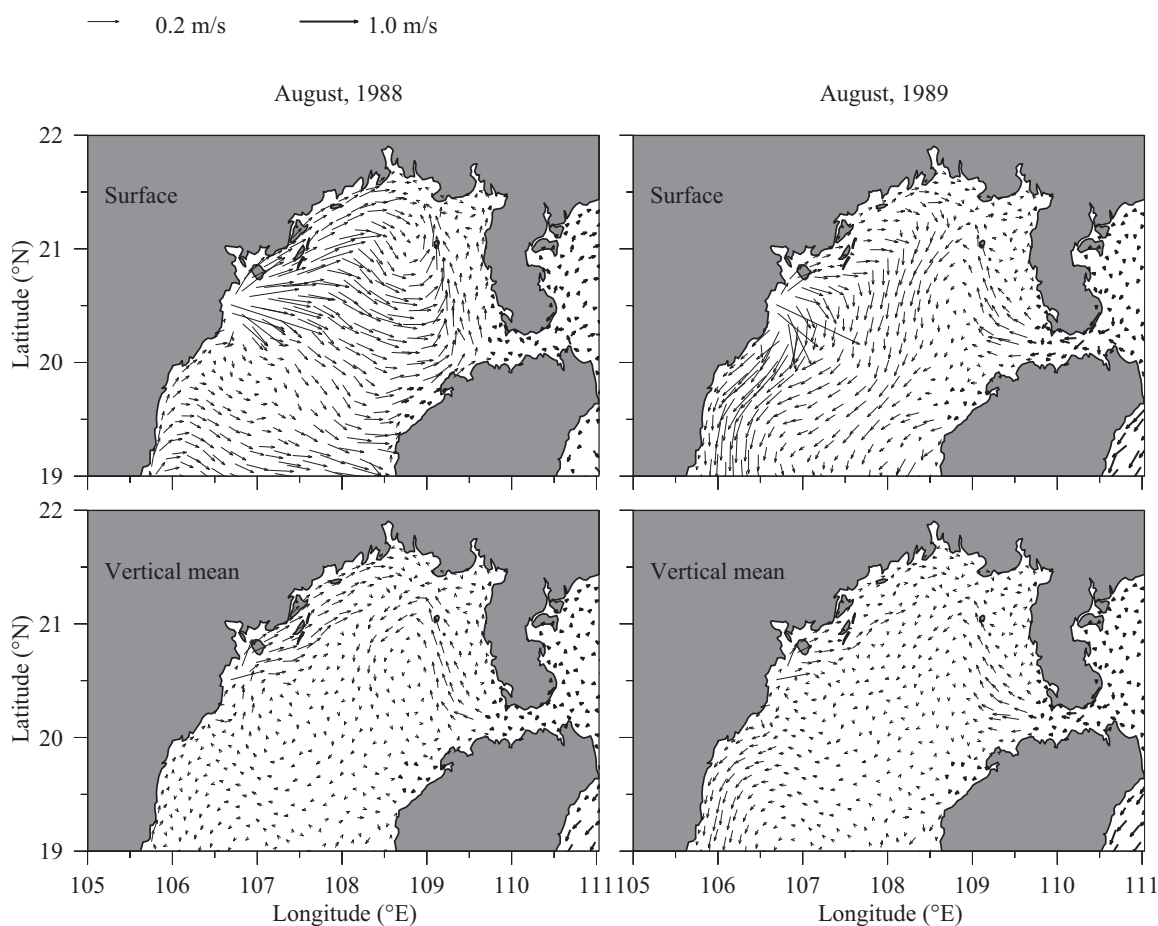
Figure 14. Maps of Global-FVCOM-computed (top) monthly averaged surface and (bottom) vertically averaged current vectors in the northern Gulf of Tonkin for August 1988 and 1989.
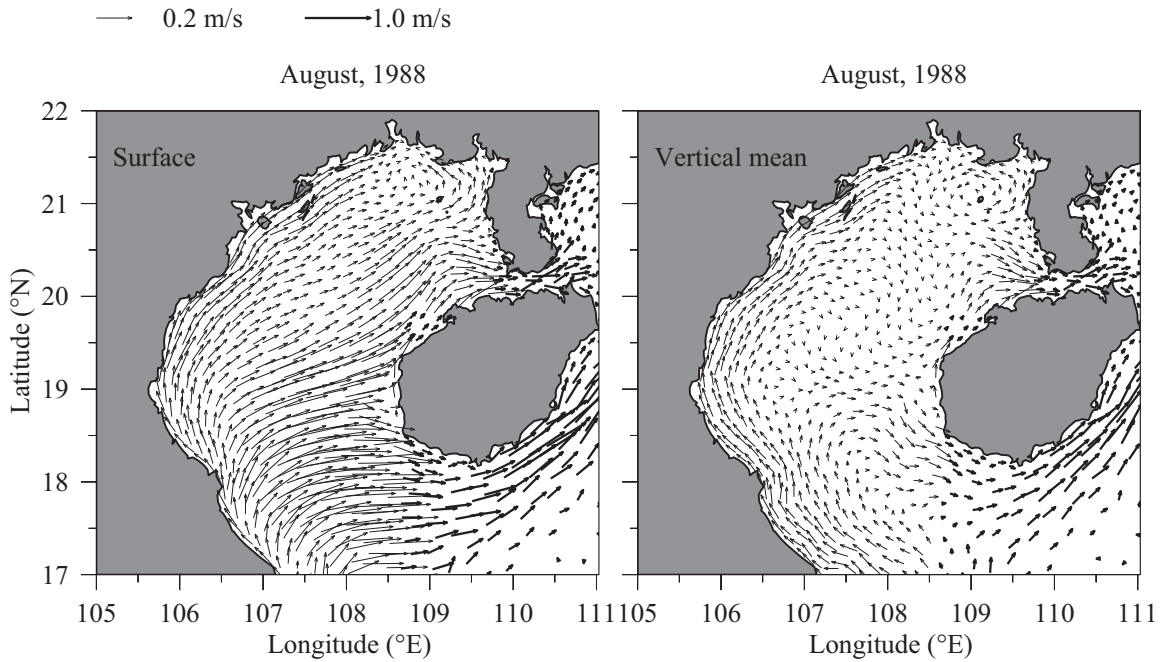
Figure 15. Maps of Global-FVCOM-computed August (left) monthly averaged surface and (right) vertically averaged) current vectors in the Gulf of Tonkin for the homogenous case with only wind forcing (Ex1).

[29] In Ex4, after adding tidal forcing into Ex3, the surface northward flow around the 20 m isobath in the eastern shelf of the northern Gulf of Tonkin was clearly intensified by the addition of tidal-rectified flow from Qiongzhou Strait (Figure 17: top right map). As a result, the vertically averaged northward flow of the cyclonic circulation in the northern Gulf of Tonkin intensified around the 20 m isobath (Figure 17: bottom right map). On the same time, the wind-induced northward flow on the western shelf moves offshore around 20°N and turns clockwise to join the cyclonic circulation in the interior.
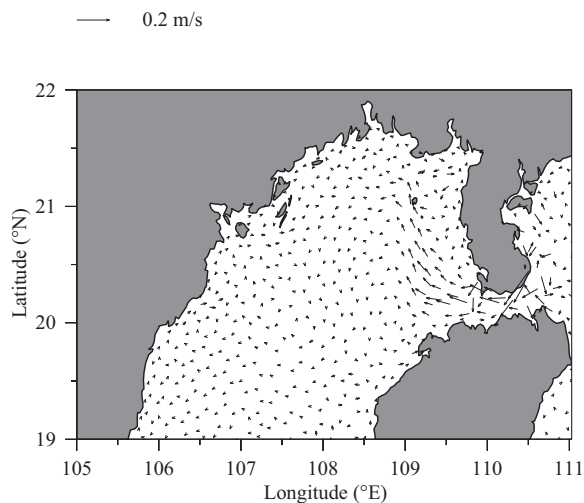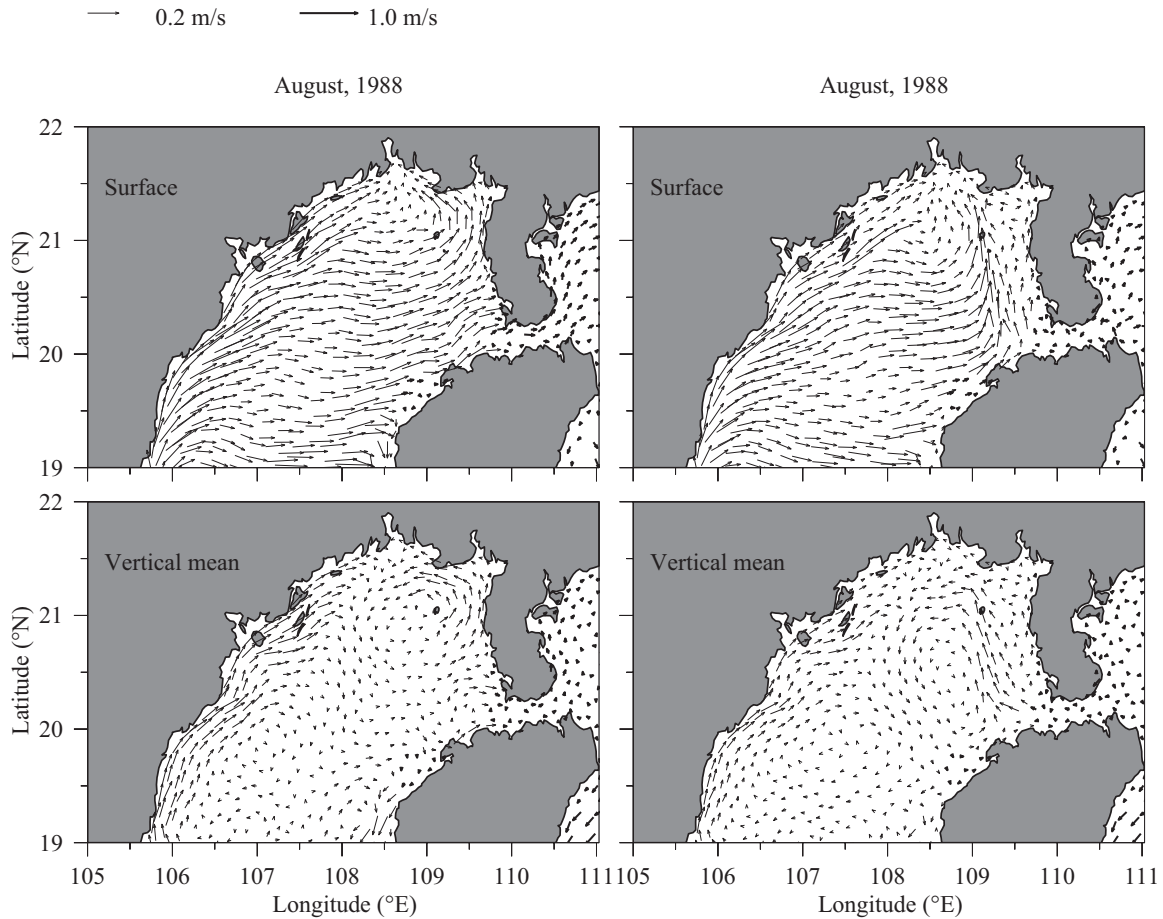

Figure 16. Maps of the monthly averaged current vectors in the northern Gulf of Tonkin for the homogeneous case with only tidal forcing (Ex 2).

[30] Combining results obtained from these four experiments clearly show that the summertime cyclonic circulation in the northern Gulf of Tonkin could form as a result of either tidal-rectified inflow from Qiongzhou Strait or the stratified wind-driven circulation. Since the water is stratified during the summer season, this summertime cyclonic circulation is a result of the combination of tidal-rectified and stratified wind-driven circulation.

[31] We also compared the results of Ex4 with the results obtained in the base model run with inclusion of river discharge. It is clear that the interaction of the southwest monsoon and buoyancy-driven flow from the Hong River significantly intensified the cyclonic circulation near the surface in the northern Gulf of Tonkin, but its contribution to the vertically averaged transport of the cyclonic circulation was not significant. Intensified northward coastal flow over the western shelf in the case with river discharge contributed more water into the northern region of the cyclonic circulation but could weaken the eastward flow in the southern region of the cyclonic circulation.

5. Summary

[32] Analysis of moored current measurements made at site A in the northern Gulf of Tonkin during October 1988 to September 1989 is presented. Rotary spectra were calculated to identify prominent energy signals and frequencies. Harmonic analysis and the band-passed filtered complex demodulation method were performed to examine the characteristics and variability of both barotropic and internal tidal currents. The correlation coefficient between 33 h low-passed subtidal current and rotated wind was estimated to quantify the role of wind forcing in the seasonal variability of the circulation in the Gulf of Tonkin. The observed

14

→ 0.2 m/s   ⟶ 1.0 m/s

August, 1988   August, 1988

Figure 17. Maps of Global-FVCOM-computed August (top) monthly averaged surface and (bottom) vertically averaged current vectors in the northern Gulf of Tonkin for the stratified cases (left) with only wind forcing and (right) with wind plus tidal forcing.

currents were compared with Global-FVCOM-computed currents, and process-oriented experiments were made using the validated Global-FVCOM to study the physical mechanism that drives the summertime cyclonic circulation in the northern Gulf of Tonkin.

[33] Rotary spectra show that the northern Gulf of Tonkin was featured by diurnal and semidiurnal tidal currents. The band-passed complex demodulation results indicated that magnitudes of tidal currents varied significantly with seasons: more energetic in the stratified summer than in the vertically well-mixed winter. The correlation coefficient between subtidal currents and surface wind was high during the winter but low during the summer. The wintertime currents showed a clockwise rotation with water depth, illustrating the nature of the wind-driven flow near the surface and Ekman spiral in the vertical. This flow structure was consistent with the cyclonic circulation pattern proposed based on barotropic wind-driven theory in previous studies. The summertime currents in the northern Gulf of Tonkin, however, were predominately northwestward or westward, contrary to the conceptual summertime circulation pattern based on wind-driven theory.

[34] The Global-FVCOM-computed currents were in good agreement with the currents recorded in 1988–1989 at mooring A. The model results indicate that the northern Gulf of Tonkin features a cyclonic circulation in both winter and summer seasons. This model-computed flow pattern was similar to the conceptual wind-driven circulation pattern in the winter season but opposite in the summer season. Process-oriented experiments showed that a summertime anticyclonic circulation could appear only with wind forcing without stratification. The summertime cyclonic circulation in the northern Gulf of Tonkin could form as a result of either tidal-rectified inflow from Qiongzhou Strait or stratified wind-driven circulation. Due to the stratified nature in the summer season, the summertime cyclonic circulation was a result of the combination of tidal-rectified and stratified wind-driven circulation.

[35] Within the East-Asian monsoon regime, the freshwater discharge from the Hong River was largest during the summer season. In general, the river runoff flow, after entering the western shelf of the Gulf of Tonkin, turned anticyclonic and flows southward along the coast. Since the bathymetry in the northern region is relatively flat, the river plume water could turn cyclonically northward with southwest monsoon forcing during the summer season. The interaction between the southwest monsoon and buoyancy-driven flow from the Hong River can significantly intensify the cyclonic circulation near the surface, but made only a small contribution to the vertically averaged flow of the cyclonic circulation.

References

Bao, X., Y. Hou, C. Chen, F. Chen, and M. Shi (2005), Analysis of characteristics and mechanism of current system on the west coast of Guangdong of China in summer, *Acta Oceanol. Sin.*, *24*, 1–9.

Beardsley, R. C., and L. K. Rosenfeld (1983), Introduction to the CODE-1 moored array and large-scale data report, in CODE-1: Moored Array and Large-Scale Data Report, edited by L. K. Rosenfeld, *Woods Hole Oceanogr. Inst. Tech. Rep. WHOI-83-23, CODE Tech. Rep. 21*, pp. 1−16, Woods Hole Inst. of Oceanogr., Woods Hole, Mass.

Chen, C., R. O. Robert, and W. D. Nowlin Jr. (1996), Near-inertial oscillations over the Texas-Louisiana shelf, *J. Geophys. Res.*, *101*(C2), 3509–3524, doi:10.1029/95JC03395.

Chen, C., H. Liu, and R. C. Beardsley (2003), An unstructured, finite-volume, three-dimensional, primitive equation ocean model: Application to coastal ocean and estuaries, *J. Atmos. Oceanic Technol.*, *20*, 159–186, doi:10.1175/1520-0426.

Chen, C., R. C. Beardsley, and G. Cowles (2006a), An unstructured grid, finite-volume coastal ocean model (FVCOM) system, *Oceanography*, *19*, 78–89, doi:10.5670/oceanog.2006.92.

Chen, C., R. C. Beardsley, and G. Cowles (2006b), *An unstructured grid, finite-volume coastal ocean model-FVCOM user manual*, 2nd ed., Tech. Rep. SMAST/UMASSD-06-0602, 318 pp., Sch. for Mar. Sci. and Technol., Univ. of Mass.-Dartmouth, New Bedford.

Chen, C., G. Gao, J. Qi, A. Proshutinsky, R. C. Beardsley, Z. Kowalik, H. Lin, and G. Cowles (2009), A new high-resolution unstructured-grid finite-volume Arctic Ocean model (AO-FVCOM): An application for tidal studies, *J. Geophys. Res.*, *114*, C08017, doi:10.1029/2008JC004941.

Chen, C., Z. Lai, R. C. Beardsley, Q. Xu, H. Lin, and N. T. Viet (2012a), Current separation and upwelling over the southeast shelf of Vietnam in the South China Sea, *J. Geophys. Res.*, *117*, C03033, doi:10.1029/2011JC007150.

Chen, C., R. L. Limeburner, G. Gao, Q. Xu, J. Qi, P. Xue, Z. Lai, H. Lin, R. C. Beardsley, and B. Owens (2012b), FVCOM model estimate of the location of Air France 447, *Ocean Dyn.*, *62*(6), 943–952, doi:10.1007/s10236-012-0537-5..

Chen, J., D. Wang, S. Ping, and Y. Du (2007), A survey of baroclinic tides in the Beibu Gulf in the South China Sea, *Acta Oceanol. Sin.*, *26*(4), 7–19.

Crosby, D. S., L. C. Breaker, and W. H. Gemmill (1993), A proposed definition for vector correlation in geophysics: Theory and application, *J. Atmos. Oceanic Technol.*, *10*, 355–367.

Fang, G. (1986), Tide and tidal current charts for the marginal seas adjacent to China, *Chin. J. Oceanol. Limnol.*, *4*, 1–16.

Fang, G., Y. Kwok, K. Yu, and Y. Zhu (1999), Numerical simulation of principal tidal constituents in the South China Sea, Gulf of Tonkin and Gulf of Thailand, *Cont. Shelf Res.*, *19*, 845–869.

Gao, G., C. Chen, J. Qi, and R. C. Beardsley (2011), An unstructured-grid, finite-volume sea ice model: Development, validation, and application, *J. Geophys. Res.*, *116*, C00D04, doi:10.1029/2010JC00668.

Gonella, J. (1972), A rotary-component method for analyzing meteorological and oceanographic vector time series, *Deep Sea Res. Oceanogr. Abstr.*, *19*, 883–846.

Guan, B., and S. Chen (1961), Current system in coast of China, in *Coast Integration Survey Off China*, Reports of Integration Survey in Coast of China, Initial Report 5, pp. 1–85, Office of the State Science and Technology Commission, Beijing, China.

He, C. (1987), China Encyclopedia: Atmosphere, Oceanography, and Hydrology, pp. 17–18, China Encycl. Publ. Co., Shanghai, China.

Hu, J., H. Kawamura, H. Hong, F. Kobashi, and Q. Xie (2001), Tidal features in the China Sea and their adjacent sea areas as derived from TOPEX/POSE IDON altimeter data, *Chin. J. Oceanol. Limnol.*, *19*(4), 293–305, doi:10.1007/BF02850732.

Hu, S., C. Chen, G. Gao, Z. Lai, J. Ge, H. Lin, and J. Qi (2012), Preliminary analysis on the simulation of the East China Sea of the Global-FVCOM model, *J. Shanghai Ocean Univ.*, *21*(4), 621–629.

Kundu, P. K. (1976), Ekman veering observed near the ocean bottom, *J. Phys. Oceanogr.*, *6*, 238–242.

Lai, Z., C. Chen, R. Beardsley, H. Lin, R. Ji, J. Sasaki, and J. Lin (2013), Initial spread of 137Cs from the Fukushima Daiichi Nuclear Power Plant over the Japan continental shelf: A study using a high-resolution, global-coastal nested ocean model, *Biogeosciences*, *10*, 5439–5449, doi:10.5194/bg-10–5439-2013.

Liang, X., X. Zhang, and J. Tian (2005), Observation of internal tides and near-inertial motions in the upper 450 m layer of the northern South China Sea, *Chin. Sci. Bull.*, *50*(24), 2890–2895.

Manh, D. V., and T. Yanagi (2000), A study on residual flow in the Gulf of Tonkin, *J. Oceanogr.*, *56*, 59–68.

Mellor, G. L., and T. Yamada (1982), Development of a turbulence closure model for geophysical fluid problem, *Rev. Geophys.*, *20*, 851–875, doi:10.1029/RG020i004p00851.

Pawlowicz, R., R. Beardsley, and S. Lentz (2002), Classical tidal harmonic analysis including error estimates in MATLAB using T_TIDE, *Comput. Geosci.*, *28*, 929–937,doi:10.1016/S0098-3004(02)00013-4.

Shi, M., C. Chen, Q. Xu, H. Lin, G. Liu, H. Wang, F. Wang, and J. Yan (2002), The role of the Qiongzhou Strait in the seasonal variation of the South China Sea Circulation, *J. Phys. Oceanogr.*, *32*(1), 103–121, doi:10.1175/1520-0485.

Smagorinsky, J. (1963), General circulation experiments with the primitive equations, I. The basic experiment, *Mon. Weather Rev.*, *91*, 99–164, doi:10.1175/15200493.

Sun, H., and W. Huang (2001), Three-dimensional numerical simulation for tide and tidal current in the Beibu Gulf, *Acta Oceanol. Sin.*, *23*(2), 1–8.

Sun, Z., J. Hu, Y. Li, Z. Chen, and J. Zhu (2009), Seasonal variation of diluted water and near-shore mixed water in the northern Beibu Gulf (in Chinese with English abstract), in *Memoir of Marine Science Investigation in the Beibu Gulf*, China Ocean Press, Beijing.

Wu, D., Y. Wang, X. Lin, and J. Yang (2008), On the mechanism of the cyclonic circulation in the Gulf of Tonkin in the summer, *J. Geophys. Res.*, *113*, C09029, doi:10.1029/2007JC004208.

Wyrtki, K. (1961), Physical oceanography of the Southeast Asian water, in *NAGA Report, Scientific Result of Marine Investigation of the South China Sea and Gulf of Thailand 1959–1961*, vol. *2*, pp. 155–160, Scripps Inst. of Oceanogr., La Jolla, Calif.

Xu, X., Z. Qui, and H. Chen (1980), Summary of the horizontal circumcurrent in South China Sea (in Chinese with English abstract), in *Chinese Society of Oceanology and Limnology, Proceedings of the Hydrology and Meteorology*, pp. 137–145, Sci. Press, Beijing.

Yang, S., X. Bao, C. Chen, and F. Chen (2003), Analysis on characteristics and mechanism of current system in west coast of Guangdong Province in the summer (in Chinese with English abstract), *Acta Oceanol. Sin.*, *25*(6), 1–8.

Yuan, S., X. Xu., J. Deng, and Z. Qiu (1995), A numerical study on internal tides in the northeast of South China Sea (in Chinese), *Trop. Ocean*, *14*(4), 15–23.

Zhang, A., and M. Jiang (1999), An analysis on tidal current temperature and salinity at a mooring station in southwest waters to Dongsha islands (in Chinese with English abstract), *Trop. Ocean*, *18*(1), 23–30.

Zhuang, M., L. Ji, and J. Lin (1981), The winds, waves and currents in the northern South China Sea (in Chinese with English abstract), in Report of the Team of Comprehensive Research, Headquarters of South China Sea Geology Investigation, Report 1–1, pp. 1–96, Dep. of Geol., Guangzhou, China.